Towards Coupling of Comprehensive Analysis into Design Sizing of a High-Speed Asymmetric Compound Helicopter

Ananth Sridharan [*] Bharath Govindarajan [†] V. T. Nagaraj [‡] Inderjit Chopra [§]

Alfred Gessow Rotorcraft Center, Department of Aerospace Engineering
University of Maryland, College Park, MD, 20742, USA

ABSTRACT

This paper investigates design trends and performance trade-offs for a lift- and thrust-augmented asymmetric single main rotor helicopter. The goal is to match the payload and range of a conventional medium-lift utility helicopter, but with an increased cruise speed of 240 knots. This configuration is compared to a thrust-augmented single rotor with a wing and a thrust-augmented coaxial design. A multi-stage multi-fidelity design framework (HYDRA) was used to sweep over the entire design space to arrive at the best vehicle design. The framework first employs simple energy based equations to calculate rotor power and drag to eliminate infeasible designs. Feasibe designs are then resized using comprehensive analysis to predict rotor performance in high-speed flight. The latter step, while relatively slower, still executes within minutes and incorporates physics-based rotor performance models without apriori tuning of power factors and other coefficients. This study presents an approach to reconcile aspects of blade flap dynamics for performance and sizing. Using this methodology, it was found that for the asymmetric compound slowed-rotor helicopter cruising at 240 knots, a stiff hingeless rotor design is required to achieve rotor trim.

INTRODUCTION

The conventional single main rotor helicopter was conceptualized as a means to achieve vertical lift, with moderate forward flight capability. At high forward flight speeds, the onset of compressibility on the advancing blade tips and airfoil dynamic stall on the retreating side introduces high vibratory loads and typically results in a higher power to operate than at lower speeds. Furthermore, the imbalance in dynamic pressure between the advancing and retreating sides of the rotor disk results in a large roll moment that might not be balanced even with full cyclic pitch control. Various aspects of rotors aeromechanics such as aerodynamics/acoustics (compressibility, reverse flow, noise), flight dynamics (rolling moment balance, autorotation), and aeroelastic effects (vibrations, stall) limit the maximum forward flight speed of a conventional single-rotor helicopter to approximately 160 knots, which falls well short of the 200+ knots envisaged for next-generation high-speed rotorcraft.

The coaxial compound and the tilt-rotor are two popular designs being pursued to achieve high-speed forward flight. While the aerodynamic efficiency of a prop-rotor installed on a tilt-rotor easily exceeds that of a rotor flying edgewise, maintenance and operating costs associated with the tilt-rotor are often significant. In a coaxial rotor system, the presence of two swashplates introduces a combination of control system complexity, excessive mast drag and/or hub weight penalties due to high blade flap stiffness requirements (driven by allowable inter-rotor tip clearances). Instead of the coaxial or tilt-rotor configurations, this paper investigates a third option for a platform with simultaneous efficient VTOL capability and high-speed cruise: the so-called lift-offset single main rotor with lift and thrust compounding.

The proposed rotorcraft configuration is an evolution of the conventional single main rotor/tail rotor helicopter. Lift and thrust augmentation devices are functionally near-identical to the coaxial compound system. The key distinguishing feature is the use of an *asymmetric fixed wing* in place of another *rotor* to balance the hub rolling moment, as shown in Fig. 1. The advantages of this configuration are :

1. **Slowed main rotor**: at high forward flight speeds, compressibility drag on the advancing blade tips is a major concern for both performance and hub vibrations. By reducing or eliminating the source of the loading, the associated penalties are minimized.

2. **Asymmetric fixed wing**: at high forward flight speeds, the fixed wing on the retreating side simultaneously alleviates rotor thrust requirements *and* provides a counter roll moment to allow for trimmed forward flight. A movable trailing edge flap is used to regulate the lift and allows for smooth variation over a range of flight speeds.

3. **Swiveling tail rotor**: At 100 knots, the anti-torque function is transferred to the vertical fin thereby offloading

[*] Assistant Research Scientist, E-mail: ananth@umd.edu
[†] Assistant Research Scientist
[‡] Senior Research Scientist
[§] Distinguished University Professor
Presented at the 42nd European Rotorcraft Forum, Lille, France, September 5–7, 2016.

the tail rotor, which can be swiveled to operate as a propeller. Once swiveled, the propeller is powered by the engine to provide propulsive thrust. Because the tail rotor functions as a propeller, the main rotor can be used to provide a pure vertical thrust (rotor shaft tilt avoided) in high-speed forward flight, thereby avoiding excessive parasitic power penalties associated with fuselage drag at high angles of attack.

PREVIOUS WORK

The field of helicopter/rotorcraft conceptual design is driven by synthesis, historical data, analysis, and parametric study to find the best configuration to perform a given mission and meet the required performance specifications. The process of design is often sequential with each step being increasingly complex in terms of the fidelity of the rotorcraft dynamics models used within these tools. However, increasing the fidelity comes with a penalty of computational cost, which make it impractical at the early design stages to use "high-cost models" where numerous permutations of vehicle configurations have to be assessed to narrow down the potential design space. Therefore, design tools have used low fidelity representations to facilitate rapid application to a wide number of design parameters (e.g., rotor disk loading, rotor tip speed, etc.). As rotorcraft configurations become more involved (e.g., the addition of a wing and/or propeller), there is a need to scan a larger design space as there is now an increase in the number of design parameters, which ultimately reflect on the total cost of computation and time. Furthermore, there is also a need to develop an accurate physics-based design tool that is capable of capturing the underlying physics of compound rotorcraft.

Various design codes exist in literature and have been widely used by helicopter industries and universities, including NDARC (NASA), RDM (Sikorsky), PRESTO (Bell Helicopter) and HESCOMP and VASCOMP (Boeing). These tools contain simple physics based models with empirical corrections to evaluate the various aspects of vehicle performance and to evaluate the component weights. As configurations and concepts become increasingly complex, there is a need to introduce higher-fidelity models such as comprehensive analysis tools. Some examples of these tools include CAMRAD II, RCAS, DYMORE and UMARC; see Johnson (Ref. 1) for a detailed summary. These codes have been used in various studies to analyze concepts such as slowed-rotor compounds (Ref. 2), tilting-tandem concept (Ref. 3), compound gyroplanes (Ref. 4) and rotors with individual blade control (Ref. 5). In a recent study (Ref. 6), NDARC was used to design three size-constrained high-speed compound rotorcraft: a tilt-rotor, a lift-offset compound coaxial configuration and a winged compound helicopter.

While a fair amount of literature exists on using design tools towards advanced rotorcraft configurations, there is a dearth in studies conducted towards the specific configuration of interest, i.e., a single-wing coupled with a lift-offset single rotor. A design with this configuration does exist for a small-scale unmanned air vehicle (UAV) under the name "Challis Heliplane" (Ref. 7). However, references to the Heliplane in the literature are few, and detailed aeromechanics analyses are unavailable in the public-domain. A passing mention exists in a survey of small-scale UAVs by Cai et al. (Ref. 8). Design optimization results for reducing vehicle weight for various configurations, including the Challis Heliplane, are presented in the work by Vu et al. (Ref. 4), which used a sizing analysis code and reduced-order models with analytical expressions to evaluate performance. While their design tool also contained an optimizer, the primary goal of the work was to validate the codes used against existing configurations. There was no improvements in design suggested for the configuration of interest. Sartorius (Ref. 9) and Cumbrebras and Sartorius (Ref. 10) studied a single rotor with lift-offset and a single-wing for a 5,000 kg vehicle in high speed forward flight. They were able to show that the flight envelope could be extended to over 250 knots when compared to a maximum flight speed of 150 knots for the conventional single rotor configuration. Their study, however, lacked a detailed investigation of the various design

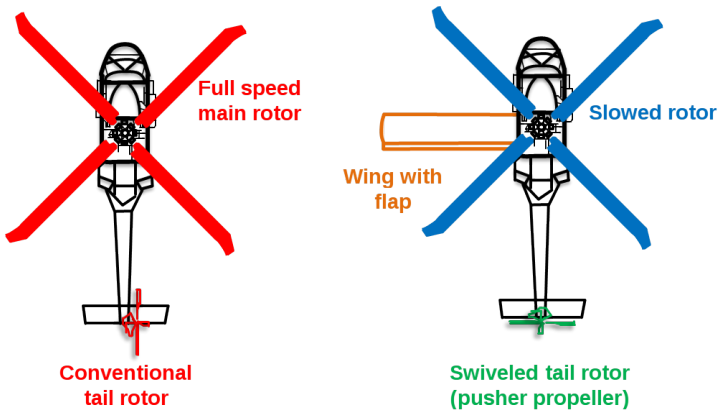

(a) Conventional Single main rotor (b) Compound

Fig. 1. Schematic representation of a baseline conventional helicopter and a compound rotorcraft with a single wing on the retreating side.

parameters and a study of the different sub-components of the vehicle at different flight conditions. The authors (Ref. 11) integrated a comprehensive analysis procedure directly into the sizing process such that the rotor drag and power were computed using higher fidelity tools such as inflow models and freewake in conjunction with simpler energy-based equations.

The objectives of this paper, and its improvements over preceding analyses is the inclusion of rotor blade deflections and trim during performance calculations. This process is a preliminary step towards integrating aspects of blade structural design into vehicle sizing by capturing the effect of flap frequency on rotor performance. The proposed methodology will directly import rotorcraft comprehensive aeromechanics analysis into the design iterations. Another objective of the paper is to demonstrate the feasibility of this framework for a medium lift GTOW for a single lift-offset rotor with a wing and propeller, a thrust-augmented coaxial compound and the winged compound as investigated by Johnson (Ref. 6).

METHODOLOGY

The developed HYbrid Design and Rotorcraft Analysis (HYDRA) tool is an integrated code suite used to perform conceptual rotorcraft design for arbitrary user-selected rotorcraft configurations. These configurations include a conventional helicopter, coaxial compound with lift and thrust augmentation, tilt-rotor, and asymmetric single rotor compounds, as shown in Fig. 2. Although initially implemented with low-fidelity performance models typical of conceptual design environments, the architecture allows for multidisciplinary design optimization. The framework was extended to encapsulate a comprehensive analysis code in the sizing process for accurate performance predictions, especially at high-advance ratios. Each component of HYDRA is described in the following section.

Helicopter Sizing

The proposed vehicle is a hybrid between a fixed-wing aircraft and a conventional helicopter. A modified sizing method based on Tishchenko's original helicopter methodology (Ref. 12) is used to size the vehicle and provide estimates of the vehicle weights and power requirements. The description of the aircraft involves defining the number of engines and lifting/thrusting components (rotors, wings and propellers), and their relative placement and orientation. A representative mission profile consisting of an idle, hover and cruise phases and the corresponding atmospheric conditions, i.e., density altitude and temperature, are used to estimate the maximum gross take-off weight, installed power and fuel required for a given payload. The sizing methodology has been validated against the NASA Design and Analysis of Rotorcraft code (NDARC) for various mission profiles, and also against various production rotorcraft (Ref. 11).

A schematic of the sizing algorithm is shown in Fig. 4. To ensure that the components contributing to aircraft empty weight are accurately represented, the weights equations presented in the NDARC (Ref. 13) are used in HYDRAs sizing tool. The equations also account for wing-related components that are sized based on structural stiffness and loading requirements. Powerplant characteristics (engine weight and specific fuel consumption) are obtained based on nominal trends for turboshaft engines. This method allows for power calculations using the comprehensive analysis during the design iterations. This inclusion of higher-order models is critical for accurate performance predictions at advance ratios of 0.5 and above, where reliable tuning factors for low-fidelity models may not be availble. For high-speed configurations, in which the main rotor operates with significant lift asymmetry between the advancing and retreating sides, a higher-fidelity flowfield model (free-vortex wake method) that is more representative of the rotor flowfield was used in the present study. The approach used by Moodie and Yeo (Ref. 14) is adopted with one key improvement; instead of repeatedly calibrating an approximate model, power is calculated using a high-fidelity analysis during sizing iterations.

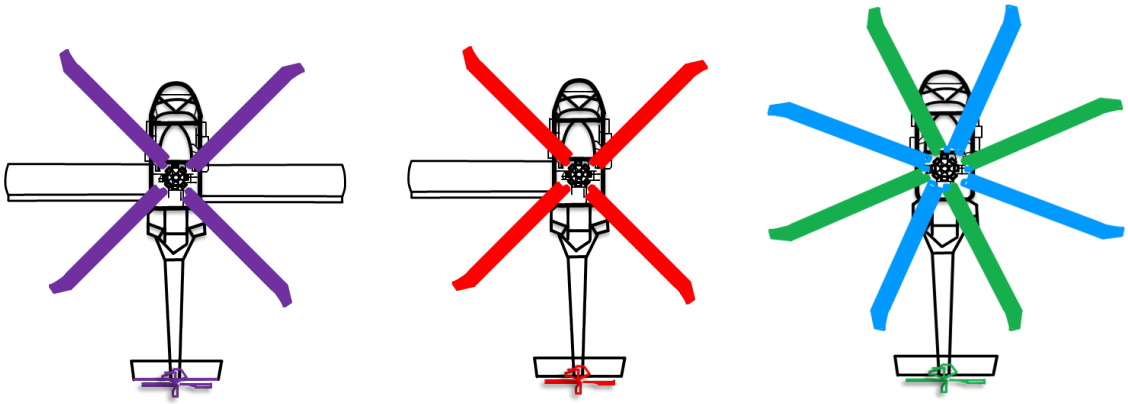

(a) Symmetric compound (full-wing) (b) Asymmetric compound (half-wing) (c) Coaxial compound (no wing)

Fig. 2. Vehicle configurations explored using the design framework, (a) Symmetric compound with full-wing, (b) Asymmetric compound with half-wing and (c) Coaxial compound.

Empty Weight

Models developed by the U.S. Army Aeroflighydynamics Directorate (AFDD) (Ref. 13) were used to evaluate the contribution of different vehicle components to the empty weight. These weights are compiled from existing helicopters and tiltrotors, from which parametric equations were extracted; these calibrated trends were then used to predict the respective component weights. The horizontal and vertical tail areas are scaled linearly with rotor radius, calibrated to the UH-60A. Engine weight is scaled linearly with the power required using the UH-60A as a reference, i.e.,

$$\text{Engine Weight} = \frac{450 \text{ lb}}{1,620 \text{ SHP}} \times \text{Installed Power, HP.}$$

Table 1: Constituent Components of Empty Weight

Group Name	Description	Dominant Dependencies
Fixed wing	AFDD93	Weight, aspect ratio
Rotor	AFDD00	Radius, solidity, flap frequency
Empennage	Custom	Radius
Propeller	AFDD82	Vehicle drag
Fuselage	AFDD82	Weight, radius
Alighting gear	AFDD82	Weight
Engine	Custom	Maximum power
Air induction	AFDD82	Engine weight
Fuel system	AFDD82	Fuel flow rate
Drive system	AFDD00	Max torque, rotor weight
Flight control	AFDD82	Rotor geometry
Deicing	AFDD	Rotor geometry

A list of the different weight groups along with their dominant dependencies are listed in Table 1. These dominant dependencies reflect the most sensitive parameters of a given empty weight group. The AFDD weight models allows for "technology factors" which, in effect reduce the empty weight by a chosen factor in anticipation of the advancement of technology over the future years. However, in the present study, all technology factors were all set to 1.0, i.e., no assumption was made for a decrease in weight based on future technologies. Therefore, the empty weight obtained through this procedure is a conservative estimate, in that is representative of current manufacturing proficiencies.

Power Calculations: Simplified Model

During design iterations, two models of different fidelity levels are available for the estimation of rotor shaft torque and engine power. The reduced-order model, implemented using momentum theory and an energy approach, does not explicitly model local effects such as varying blade geometry, tip compressibility or stall. Instead, these losses are folded into power factors that multiply the induced and profile power coefficients; see Ref. 11.

Engine Installed Power The transmission output power is the sum of the power required to rotate the main rotor(s), tail rotor and propeller (if present). Transmission and engine air intake efficiencies, together with temperature/altitude compensations are applied to evaluate to the engine installed power in each mission segment. The maximum installed power and maximum torque are used in the AFDD/NDARC empty weight models to estimate the empty weight contributions from the drive system and air induction groups.

Role of Blade Dynamics The natural flap frequency of the rotor blade is an important design parameter that has a significant impact on overall rotor and vehicle take-off weight and power. This parameter was originally introduced as a design driver in sizing analysis tool to account for variations in rotor hub designs. For instance, compared to articulated systems, hingeless blades are stiffer (and therefore heavier) to withstand higher bending stresses. This increase in blade weight results in higher hub weight (needed to carry larger centrifugal loads). The increased rotor group weight eventually cascades into other aspects of empty weight, eventually driving up take-off weight (Ref. 11).

Even though a stiffer rotor results in a heavier rotorcraft, the advantages of such a design for high-speed configurations outweigh the potential shortcomings. Typically, an articulated system may not be able to operate at very high-advance ratios. The combination of reduced rotor RPMs and large variations in dynamic pressure over the azimuth may result in large blade flap motions and even tunnel strike. Further, some of the rotor energy is dissipated through aerodynamic flap damping, resulting in potentially reduced aerodynamic efficiency and increased fuel consumption for articulated systems. Hingeless blades with high flap frequency may provide the structural stiffness required to carry the transient loads at high advance ratios, and minimize energy loss due to blade flapping.

Because of these considerations, it is important to accurately reflect the physics of blade flapping during performance calculations. In the present work, the flap frequency in hover is prescribed as an input parameter. The hinge offset and root flap spring stiffness are obtained as follows:

1. The expression for flap natural frequency of a rotor blade is:

$$\nu_\beta^2 = 1 + \frac{3e}{2(R-e)}$$

This expression can be rearranged to compute hinge offset as

$$e = 2R(\nu_\beta^2 - 1)\left[3 + 2(\nu_\beta^2 - 1)\right]^{-1} \quad (1)$$

If the prescribed flap frequency can be achieved with 5% hinge offset or less, then the flap spring stiffness is set to zero, and hinge offset is determined according to Eqn. 1. This limit corresponds to a flap frequency of 1.039/rev.

2. If the prescribed flap frequency is above 1.039/rev, i.e., if more than 5% hinge offset is required, then the hinge offset is set to 5%, and a root flap spring is added to augment the stiffness and achieve the target frequency. In this case, the spring stiffness is calculated from the following expression for flap natural frequency with a root spring:

$$\nu_\beta^2 = 1 + \frac{3e}{2(R-e)} + \frac{K_\beta}{I_\beta \Omega^2}$$

Substituting for $e = 0.05R$, the flap spring stiffness can be computed as

$$K_\beta = \left(\nu_\beta^2 - 1 - \frac{3e}{2(R-e)}\right) I_\beta \Omega^2$$

The blade flap inertia is computed assuming uniform mass distribution along the blade, and blade mass is computed using the AFDD00 empty weight model.

The fundamental flap mode is used in the comprehensive analysis with airfoil tables to compute rotor performance in wind-tunnel trim mode at high advance ratios. Accounting for blade motions allows for studying trade-offs between total vehicle take-off weights and power required.

Practical Limits The rotor power calculations in the modified disk model do not take into account local effects like airfoil static stall and advancing blade stresses. Therefore, depending on the choice of input variables (rotor solidity, tip speed and disk loading) the simplified performance calculations will fail to identify designs which are not practical. To filter out designs which require unrealistic values of rotor thrust, two simple thresholds are set to identify unrealistic configurations:

1. **Hover blade loading:** When the hover blade loading coefficient C_T/σ is above 0.13, the mean operating lift coefficient of the rotor sections is 0.78. Depending on the twist and chord distribution of the rotor sections, certain sections may operate close to stall, leaving little margin for maneuvers or gust tolerance. Therefore, designs that exceed this threshold are discarded.

2. **Lift offset:** Rotor lift offset is a non-dimensional metric that represents the lateral bias of average vertical thrust towards the advancing side with respect to the shaft. For a coaxial system, individual rotors may be trimmed to the same lift offset, producing mutually canceling hub rolling moments. For the asymmetric compound design, the lift offset is obtained from the body rolling moment balance.

   It can be shown from aerodynamic considerations (Ref. 11) that, based on qualifying assumptions, the lift offset ranges from 0.125 $\mu^3/(1\text{-}0.25\mu^2)$ to $4/3\pi$, with an expected value of $4\mu^3/(3\ \pi\ (1\text{-}0.5\mu^2))$. For the current mission, the cruise advance ratio is approximately 0.75, setting the limits at 0.061 and 0.42, with an expected value of 0.125.

   A rotor with a lift-offset greater than 0.5 is required to produce most of its thrust from the outboard sections on advancing blades, resulting in enormous bending loads and associated hub rolling moment. The lower limit 0.1 is set based on the expected value, and 0.5 is set as an inclusive upper bound. These values are inclusive in that they serve to only filter out designs that are clearly infeasible for high advance ratio flight.

3. When comprehensive analysis is used to predict rotor performance during sizing iterations, the trim process does not converge for some combinations of rotor flight and thrust conditions. In these cases, the power required for such un-trimmable configurations is increased by an additional 1000 Hp to penalize these designs. Further, when the blade coning, lateral or longitudinal flap angles exceed 12 degrees, or if the rotor system cannot achieve trim, the designs are similarly penalized.

With impractical designs filtered out based on hover blade loading and lift offset (for the asymmetric compound), the configurations that "pass" this test are resized based on power predictions from the comprehensive analysis. This methodology is schematically shown in Fig. 3.

Comprehensive Analysis

An in-house comprehensive structural dynamics (CSD) analysis was developed based on a doctoral dissertation (Ref. 15), which was also used in CFD-CSD coupling studies (Ref. 16). This solver is used to model the rotor aerodynamics. Blade section aerodynamic forces are obtained using table look-up for Mach number and angle of attack. The inflow calculation can be performed either using the Peters–He dynamic inflow model (Ref. 17) or the Maryland Free-vortex Wake model (MFW) (Ref. 18). When the free wake model is used, alternate updates of wake geometry and trim controls are performed until the rotor swashplate inputs converge across fixed-point iterations.

Power Calculation with Comprehensive Analysis: The comprehensive analysis code is used to evaluated rotor power requirements in cruise. The high-fidelity model is executed in

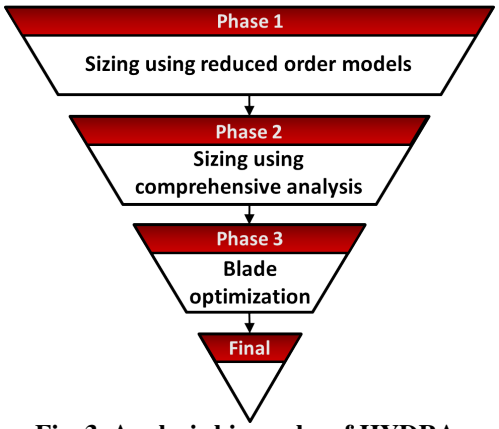

Fig. 3. Analysis hierarchy of HYDRA.

wind-tunnel trim mode, and the collective and cyclic pitch angles are iteratively adjusted to match the target time-averaged rotor thrust and hub pitching and rolling moments. The rotor shaft angle is set to 0.5 deg aft with respect to the freestream. Blade flap motions for the cases considered are included to capture the role of flap damping on rotor power required, and to ensure that rotor deflections are accurately represented during the design process. Rotor disk loading and take-off weight are used to prescribe the radius, and the tip speed is used to set the rotor RPM. A uniform chord distribution is prescribed based on blade aspect ratio with 15% root cut-out. The SC1095 airfoil tables are used to compute sectional lift and drag coefficients for various combinations of angle of attack and Mach number. Once wind-tunnel trim is achieved, the hub drag force $F_{x,H}$ and shaft power P_{cr} are extracted from the outputs and used to compute the mechanical power required to rotate the rotor(s) and propeller.

RESULTS

A representative mission was chosen for the evaluation of the designs and the mission parameters chosen to size the vehicle are given in Table 2. Design parameters and their respective ranges of values investigated in the present work are given in Table 3.

Table 2: Cruise mission profile

Mission parameter	Value	Units
Atmosphere	ISA + 5	°C
Hover altitude	2000	meters
Cruise altitude	1500	meters
Hover duration	5	minutes
Cruise speed	240	knots
Payload	2000	kg
Range	450	n.mi

Table 3: Design parameters and their ranges

Rotor parameter	Range	Units
Disk Loading DL	6 – 18	lb/sq.ft
Rotor Solidity σ	0.06 – 0.14	
Number of blades N_b	4	
Hover tip speed V_{TIP}	240	m/s
Cruise tip Mach limit	0.5 – 0.9	
Wing parameter	**Range**	**Units**
Aspect ratio AR	4 – 10	
Lift fraction f_W	0 – 0.5	

In previous work (Ref. 11), the effect of number of blades was found to play a minor role on overall sizing compared to rotor solidity and disk loading. Therefore, the number of blades per rotor in each rotor is frozen at 4 for the present study. Additionally, a higher hover tip speed is necessary to allow for sufficient stall margin. Therefore, the hover tip Mach number at sea level is frozen at 0.7, i.e. V_{TIP} = 240 m/s. Further, a linear blade nose-down twist of 10 deg was found to reduce rotor power requirements in cruise for a heavily loaded rotor. In contrast, blade twist did not affect vehicle sizing when the rotor is off-loaded by the fixed wing(s). Therefore, all design iterations with comprehensive analysis in-the-loop were carried out with 10 deg of blade twist.

Three helicopter configurations are compared in this study: a thrust-augmented coaxial compound configuration, an asymmetric compound helicopter and a lift-and-thrust augmented single rotor helicopter. The coaxial configuration does not feature fixed wings and relies on the rotors to carry the entire weight in cruise. In contrast, the single rotor configurations exhibit significant thrust alleviation (35 - 40%) through use of fixed wing(s). For the configuration with symmetric fixed wings, the rotor is trimmed to zero lift offset, i.e. zero rolling moment.

The phase-1 results were obtained using the reduced order model (ROM) which features simple equations for power based on energy relations and augmented with empirical corrections. The minimum fuel design was identified based on parametric sweeps using 20,000 combinations of the design variables given in Table 3. These configurations ("potential designs") were obtained by filtering out converged designs based on both hover blade loading C_T/σ and rotor lift offset in cruise. Rotor lift offset is restricted to values from 0.1 to 0.42 for the asymmetric compound (Ref. 11). The vehicle specifications for this minimum fuel design are given in the first three columns of Table 4.

With the simple model, the flap natural frequency at hover is set to 1.05/rev for the single rotor configurations, and to 1.35/rev for the coaxial rotor to avoid blade strike. Parametric sweeps were conducted for all three designs. In the modified disc model, the rotor induced power factor (shown in Fig. 7) is capped at 4.5 when the advance ratio exceeds $\mu = 0.5$ based on previous work (Ref. 11). The results obtained from rotorcraft sizing with this imposed upper limit on rotor inefficiency are labeled "modified disk model". If the original trendline is extrapolated to higher advance ratios, the associated errors in performance calculations cascade into all aspects of sizing, resulting in significant increases in empty weight and fuel required.

As predicted by the modified disk model, the gross take-off weights, rotor solidities, empty weight, installed power, fuel required and hover blade loading for all configurations investigated are quantitatively similar, i.e. within 4% of each other. This performance model drives the design towards a higher advancing tip Mach number (0.8) to reduce rotor induced power in cruise. Rotor lift offset for the coaxial compound and the asymmetric compound are also similar.

Quantitative inferences of relative performance comparisons between the the three compound rotorcraft as predicted by the modified disk model can be misleading owing to inherent assumptions in its formulation that may break down in high speed (and high advance ratio) flight. At this flight condition, the advance ratio μ is approximately 0.75. Therefore, the design sweep was performed using the blade element analysis with a rigid rotor system to evaluate rotor performance and resize all three vehicles. The results of this study are presented in columns 4, 5 and 6 of Table 4.

For the single rotor configurations, the best design as obtained from sizing iterations with the modified disk model significantly over-predicts cruise rotor power (and therefore fuel weight) compared to the corresponding design obtained from the blade element model with airfoil tables. This comparison is evident from an examination of columns 1 through 6 of Table 4 along the highlighted row. The primary driver for this increased power requirement is the advancing blade tip Mach number in cruise. Using the simplified model, all configurations prefer an advancing cruise tip Mach number of 0.8. In contrast, the single rotor configurations as obtained from the blade element model feature an advancing cruise tip Mach number of 0.5, i.e., lower rotor RPM in cruise and reduced profile power.

One of the most significant differences between the two sets of designs obtained using different performance models is the prediction of fixed wing span and lift carried for the symmetric compound. The blade element model predicts that the wing must carry 30% more vehicle weight *over and above* the 40% predicted by the modified disk model. Correspondingly, the wing span (and wing area) required to carry this lift increases by 30%. For the asymmetric compound configuration, the minimum fuel design obtained from the blade element rigid rotor model exhibits a lower disk loading, 32% larger rotor and thus 16% more empty weight compared to the design obtained using the reduced-order performance model. Even with the heavier vehicle with correspondingly larger drag, the reduction of rotor speed in cruise significantly alleviates rotor power requirements, resulting in a net decrease in fuel required.

The modified disk model is calibrated for a high cruise blade loading similar to that of the coaxial compound rotorcraft, and so predictions of fuel required are not significantly different for that platform. For the single rotor configurations, however, the modified disk model over-predicts power required by 33%. Minimum fuel designs feature consistently higher disk loadings for the single rotor configurations and up to 17% over-prediction of installed power.

Finally, the parametric sweep was repeated for all three configurations with flap dynamics included as part of the performance calculations using rigid rotor blades, and are given in columns 7, 8 and 9 of Table 4. This step ensures that rotor trim is achieved for every potential design during the sizing iterations. The resulting designs, when sorted by fuel, automatically contain combinations of flap frequency and cruise rotor RPMs that are appropriate for achieving the loads needed to sustain flight.

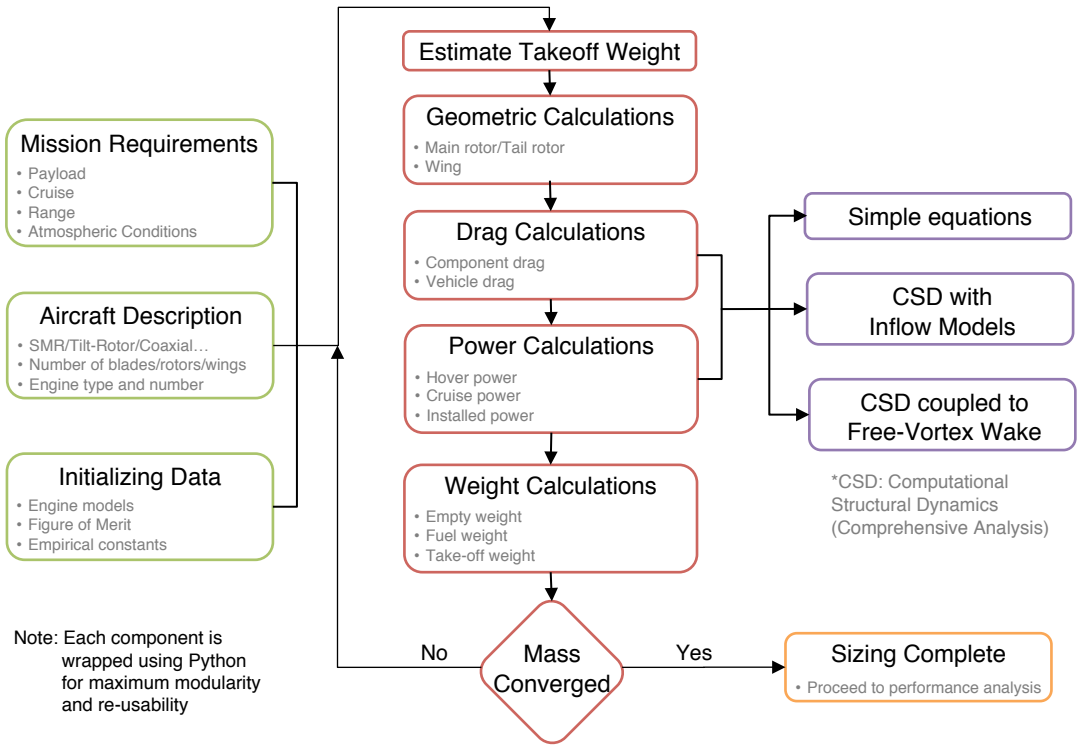

Fig. 4. Flowchart depicting the HYDRA framework.

Table 4: 240 knots design for minimum fuel

	Phase 1: Modified disk model			**Phase 2: Rigid rotor**			**Phase 3: Blade dynamics**		
Rotor parameter	1 Symmetric	2 Asymmetric	3 Coaxial	4 Symmetric	5 Asymmetric	6 Coaxial	7 Symmetric	8 Asymmetric	9 Coaxial
Number of blades, N_b	4	4	4	4	4	4	4	4	4
Disk Loading DL, lb/sq.ft	13	13	11	14	8	12	15	12	14
Solidity, σ	0.08	0.08	0.07	0.11	0.08	0.13	0.1	0.09	0.15
Flap frequency, ν_β /rev	1.05	1.05	1.35	1.05	1.05	1.3	1.10	1.20	1.35
Hover C_T/σ	0.137	0.136	0.132	0.110	0.084	0.078	0.126	0.112	0.079
Cruise tip Mach limit	0.8	0.8	0.8	0.5	0.5	0.8	0.5	0.6	0.8
Gross Weight, lbs	23,379	23,476	23,222	22,131	25,003	25,277	22,036	24,938	26,166
Fuel Weight, lbs	**3,990**	**4,010**	**4,192**	**3,043 (-24%)**	**3,063 (-24%)**	**4,051**	**3,197(-20%)**	**3,592 (-10%)**	**4,313**
Empty Weight, lbs	14,990	15,065	14,630	14,690	17,541	16,826	14,440	16,947	17,454
Installed Power, hp	5,872	5,902	6,180	5,201	4,788	6,263	5,233	5,433	6,914
Radius, ft	25.5	25.6	19.5	24.2	33.9	19.7	23.3	27.7	18.5
Lift Offset	0.00	0.30	0.27	0.00	0.22	0.27	0.00	0.37	0.30
Wing parameter	1 Symmetric	2 Asymmetric	3 Coaxial	4 Symmetric	5 Asymmetric	6 Coaxial	7 Symmetric	8 Asymmetric	9 Coaxial
Aspect ratio AR	9	9	–	9	6	–	9	7	–
Span, ft	22.1	29.3	–	28.7	27.6	–	30.6	30.6	–
Lift fraction f_w	0.4	0.35	–	0.70	0.35	–	0.80	0.40	–

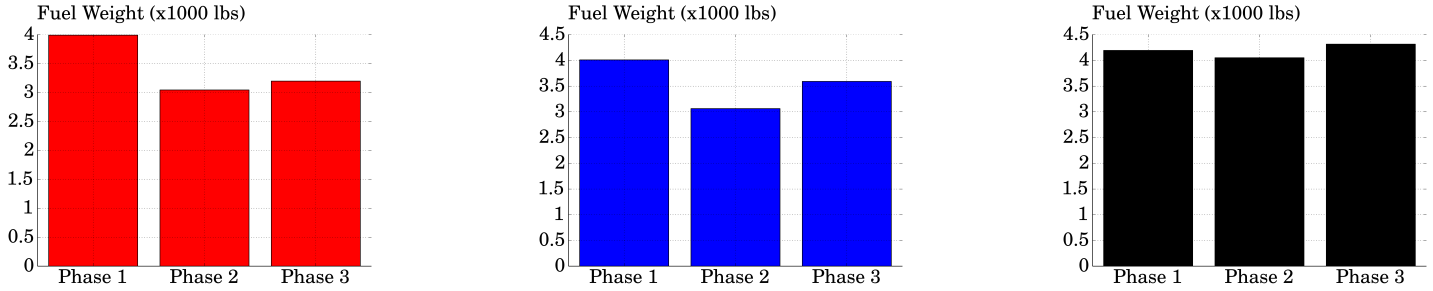

(a) Symmetric Compound (b) Asymmetric Compound (c) Coaxial Compound

Fig. 5. Fuel weight predictions for high-speed configurations with different performance model

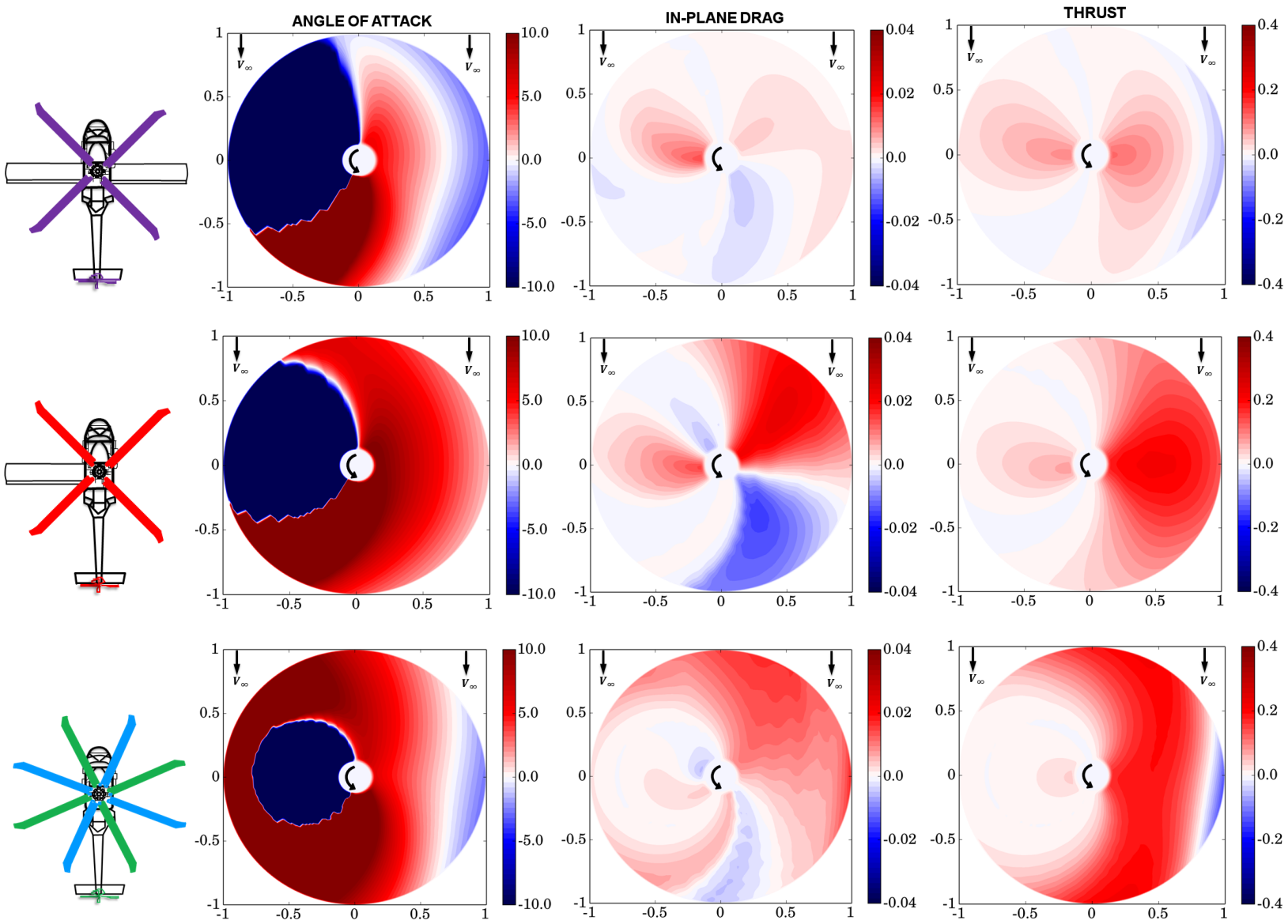

Fig. 6. Angle of attack, in-plane drag and thrust distribution for minimum fuel designs at 240 knots with rigid blade flap dynamics.

For the symmetric compound configuration, the effect of including blade flap dynamics is seen by comparing columns 4 and 7. Fuel requirements increase by 5% due to energy dissipation through flap damping. Further, the fraction of weight carried by the wing in cruise increases from 70% to 80%, and the span grows correspondingly. A higher disk loading results in a more compact rotor system (4% less diameter). The empty weight and fuel weight are near identical for both designs. The effect of higher disk loading on installed power is offset by 10% reduction in solidity, and so the installed power is not significantly affected.

To obtain rotor trim for the lift-offset asymmetric compound configuration, numerical studies showed that the flap frequency must be at least 1.2/rev. The minimum fuel design features a higher disk loading (and therefore smaller radius) and larger rotor solidity compared to that obtained without rotor blade flapping, resulting in marginal changes in empty weight. Wing lift contribution to overcoming gravity increases from 35% to 40%, resulting in a larger span and increased lift offset. The combination of higher disk loading and larger solidity results in negligible changes in installed power. However, the cruise efficiency of the system degrades because of the higher advancing tip Mach number required to achieve rotor trim, resulting in 17% increase in fuel required.

For the coaxial compound, the minimum fuel design features a higher disk loading and larger solidity compared to the designs obtained from the first two performance models. This compact rotor system contributes towards reductions in empty weight, but these reductions are offset by the weight increases due to higher flap frequency. If the root spring stiffness is not set to match a flap frequency of 1.3/rev, then rotor trim cannot be achieved for the heavily loaded coaxial rotor. However, with the blade flap dynamics included, only configurations with a cruise tip Mach number of 0.8 could achieve wind-tunnel trim at 240 knots. This increased rotor tip speed results in a large build-up of compressibility drag on the advancing side and 6.5% more fuel.

The modified disk model fails to predict rotor performance accurately, especially for lightly loaded conditions at high speeds. Depending on the calibrated thrust condition, it may either over-predict or under-predict power required, which cascades into sizing the rest of the rotorcraft. The rigid rotor blade element model under-predicts power required, and does not capture energy loss due to flap damping or loss of vertical thrust due to excessive flap angles. Inclusion of blade flap dynamics in performance during sizing iterations is critical to accurately reflect the role of the flap frequency in helicopter sizing. The approach presented above is one method to study the trade-offs between rotor weight and performance improvements due to blade stiffness.

Comparison of Lift and Drag Distribution

Figure 6 shows plots of the operating angles of attack, in-plane chordwise force and vertical thrust distribution over the rotor disk at 240 knots cruise for each of the three designs: symmetric winged compound, asymmetric compound and thrust-augmented coaxial helicopter. The rotor in the symmetric winged compound design is lightly loaded and carries only 20% of the vehicle weight, rotates at 20% hover RPM and requires only 21 Hp to rotate the shaft. The advance ratio is μ=2.64 for this flight condition. Owing to the reduced rotor speeds and off-loaded operating condition, the in-plane drag was found to be very small compared to the other two designs. Most of the vertical thrust is carried on the advancing and retreating sides. Due to blade geometric twist, the advancing blade tips experience negative lift which helps trim the rotor to zero rolling moment.

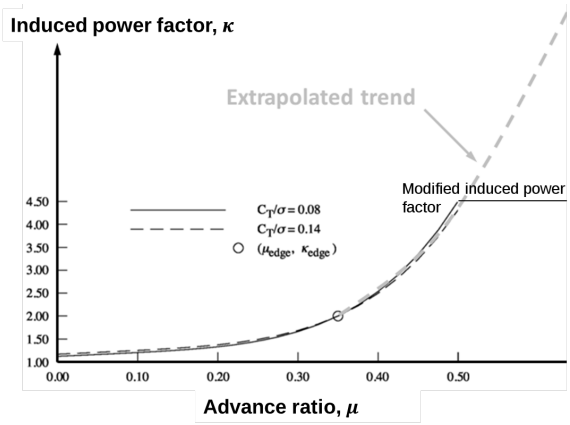

Fig. 7. Variation of rotor induced power factor κ with Advance Ratio μ (Ref. 13).

In the asymmetric compound configuration, the rotor carries 60% of the vertical thrust, with the remaining 40% offloaded to the fixed wing. In high-speed cruise, the operating advance ratio is μ=1.53, the rotor rotates at 33% hover RPM and requires 167 Hp to produce the desired thrust. Most of the shaft torque reduction due to aft tilt in high-speed flight is offset by increased hub drag. The rotor is trimmed to a non-zero lift offset and the fixed wing provides rolling moment balance; therefore, most of the vertical thrust is produced on the advancing side.

The coaxial compound configuration operates at an advance ratio of μ=0.83. The rotors rotate at 62% of the hover RPM and carry 100% of the vehicle weight. The power required to rotate both rotors in cruise is 800 hp. Most of the vertical thrust is produced on the advancing side with a small negative loading region at the blade tips at 90 deg rotor azimuth. The retreating side does not carry a significant thrust because the rotor is trimmed to a non-zero lift offset. Most of the in-plane drag (contributions to shaft power) are prevalent over the nose of the disk and on the advancing blade tips.

Tables 5 and 6 show alternative designs for the symmetric winged compound and asymmetric compound configurations, respectively. These designs were obtained with the blade dynamics included as part of the sizing process. The alternate designs are chosen based on reduced footprint, reduced takeoff weight or reduced disk loading (hover downwash velocities).

Table 5: Alternate designs for the symmetric winged compound at 240 knots cruises speed with blade dynamics.

Rotor parameter	Symmetric		
	Min Fuel	Low disk loading	Smaller footprint
Number of blades, N_b	4	4	4
Disk Loading DL, lb/sq.ft	15	12	16
Solidity, σ	0.10	0.10	0.09
Flap frequency, ν_β /rev	1.10	1.15	1.15
Hover C_T/σ	0.126	0.100	0.149
Cruise tip Mach limit	0.5	0.5	0.5
Gross Weight, lbs	22,036	24,878	21,482
Fuel Weight, lbs	3,197	3,269	3,128
Empty Weight, lbs	14,440	17,210	13,955
Installed Power, hp	5,233	5,498	5,181
Radius, ft	23.3	27.6	22.2
Lift Offset	0.00	0.00	0.00
Wing parameter	Min Fuel	Low disk loading	Smaller footprint
Aspect ratio AR	9	9	9
Span, ft	30.6	30.4	30.2
Lift fraction f_w	0.80	0.70	0.80

Table 6: Alternate designs for the asymmetric winged compound at 240 knots cruises speed with blade dynamics.

Rotor parameter	Asymmetric		
	Min Fuel	Low disk loading	Small footprint
Number of blades, N_b	4	4	4
Disk Loading DL, lb/sq.ft	12	10	15
Solidity, σ	0.09	0.08	0.10
Flap frequency, ν_β /rev	1.20	1.20	1.20
Hover C_T/σ	0.112	0.105	0.126
Cruise tip Mach limit	0.6	0.5	0.6
Gross Weight, lbs	24,938	26,740	23,895
Fuel Weight, lbs	3,592	3,706	3,851
Empty Weight, lbs	16,947	18,634	15,644
Installed Power, hp	5,433	5,440	5,672
Radius, ft	27.7	31.4	24.2
Lift Offset	0.37	0.32	0.41
Wing parameter	Min Fuel	Low disk loading	Small footprint
Aspect ratio AR	7	6	7
Span, ft	30.6	30.5	29.9
Lift fraction f_w	0.40	0.40	0.40

Phase 3: Blade Aerodynamic Design

Main rotor blade geometry design studies were performed to determine whether performance improvements could be realized for each of the three vehicle configurations. Both bilinear twist and taper were investigated in this study. Most of the performance improvements can be realized through linear twist. The baseline design with 10 deg nose down linear twist is very close to the minimum total power configuration.

Table 7: Rotor aerodynamic design parameters for coaxial configuration using two aerodynamics models.

Parameter	Baseline	Bilinear Twist	Bilinear Taper
Linear Inflow			
Twist junction	50%	30%	30%
Twist at junction	5°	−1°	−1°
Tip twist	10°	−5°	−5°
Taper junction	–	–	70%
Root chord, ft	2.18	2.18	2.18
Tip chord, ft	2.18	2.18	1.31
Power (per rotor), hp	873	831	808
Free-Vortex Wake			
Twist junction	50%	40%	40%
Twist at junction	5°	4°	4°
Tip twist	10°	11°	11°
Taper junction	–	–	50%
Root chord, ft	2.18	2.18	2.40
Tip chord, ft	2.18	2.18	1.31
Power (per rotor), hp	723	713	688

Table 8: Rotor aerodynamic design parameters for asymmetric configuration using two aerodynamics models.

Parameter	Baseline	Bilinear Twist	Bilinear Taper
Linear Inflow			
Twist junction	50%	30%	30%
Twist at junction	5°	−2°	−2°
Tip twist	10°	−2°	−2°
Taper junction	–	–	50%
Root chord, ft	1.95	1.95	1.95
Tip chord, ft	1.95	1.95	1.61
Power (per rotor), hp	776	545	544
Free-Vortex Wake			
Twist junction	50%	50%	50%
Twist at junction	5°	1.5°	1.5°
Tip twist	10°	3°	3°
Taper junction	–	–	50%
Root chord, ft	1.95	1.95	1.95
Tip chord, ft	1.95	1.95	1.75
Power (per rotor), hp	876	770	767

Parametric studies were restricted to the coaxial rotor and the asymmetric compound. The symmetric compound was also investigated, and no significant performance improvements could be realized for the lightly loaded main rotor. Tables 7 and 8 show the blade designs obtained using linear inflow and free wake that yield minimum total cruise power. In each configuration, the rotor geometric solidity is set to the corresponding value in Table 4.

For the asymmetric compound configuration, the main ro-

tor carries 60% of the total vehicle weight in cruise with 40% lift offset. Predictions from the linear inflow model show that a blade with 3 deg linear twist reduces power by 100 hp. Application of taper over and above twist does not have a significant effect on total power (3 hp). However, these power reductions are still insiginificant compared to the engine installed power (less than 2%). Predictions from the free wake model are also shown in Table 8. Compared to the baseline twist of 10 deg, the untwisted untapered blade has a power saving of 4% of installed power. Again, application of taper does not cause a significant change in cruise power required, because the advancing tip Mach number is 0.6.

For the coaxial configuration, each rotor carries 50% of the vehicle weight at 62% of hover RPM. Predictions obtained from parametric sweeps using the linear inflow model show that 5 deg of nose-down linear twist may yield marginal power savings (less than 1%), and application of taper does not significantly alter the cruise power requirements. Similar trends are observed when using the free-vortex wake model to predict rotor power. Most of the power savings are realized through application of blade twist, and taper has a marginal effect on improving cruise performance for the slowed rotor.

SUMMARY AND CONCLUSIONS

In summary, rotor dynamics at high advance ratios results in significant breakdown of underlying assumptions used in the simplified performance models. While implementation of tuned induced power factors as table look-up functions of thrust and flight conditions may circumvent the issue temporarily, including the comprehensive analysis within the design iterations as a higher-fidelity alternative avoids the problem altogether. Furthermore, the design process was found to be sensitive to the fidelity of the performance model used to compute the rotor power and torque. Significant differences in vehicle configurations were observed while using a simple reduced order model, rigid rotor and flapping blade with airfoil tables. Finally, this design tool capability presents an option to the designer to obtain rotor performance using detailed physics-based models with fewer underlying assumptions.

Sizing studies were performed in the design of a compound high-speed asymmetric compound helicopter (single wing and pusher propeller) that is capable of performing a mission similar to that of a full-scale medium lift utility helicopter, but with a cruise speed of 240 knots. An earlier numerical framework (HYDRA) was further developed and used to arrive at an optimal design for the configuration. This analysis calculates the rotor power in conjunction with either a simple energy based model, or rigid rotor with comprehensive analysis or a flapping rotor with comprehensive analysis. The designs were compared against a conventional twin-wing single main rotor and a coaxial rotor (both equipped with a pusher propeller). Based on this framework, vehicle designs were obtained for the different configurations and the following specific conclusions were drawn from this study:

1. The simpler energy-based equations for rotor power rely on empirical trends to capture physical phenomenon such as the induced power factor, which tend to erroneously over-predict or under-predict performance at high rotor advance ratios (these factors are not necessary tuned to extreme flight conditions). The performance of the rotor was better predicted using comprehensive analysis in the design loop. If these simpler equations are to be used, then these factors should be carefully calibrated for very high advance ratios for different rotor configurations.

2. The present methodology identifies several feasible designs that may be ranked by different combinations of vehicle characteristics (disk loading, fuel, take-off weight, footprint, etc) and allows greater flexibility for the designer, because postprocessing and ranking designs is decoupled from the parametric sweep (unlike optimization processes that rely on a pre-defined objective function).

3. The addition of a simple flap dynamic model in the sizing process significantly altered the final configuration of the vehicle indicating the sensitivity of the design procedure to an improved fidelity in the aerodynamic model (6% increase in gross take-off weight and 3% increase in fuel for the asymmetric compound) compared with the modified disk model.

4. To accurately capture the effects of flap frequency as a sizing parameter on blade dynamics, the root spring stiffness and hinge offset are tuned based on this rotor property and used in the dynamics. The inclusion of flapping dynamics does not significantly affect the off-loaded rotor in the symmetric winged compound, but has a significant effect on the sizing of rotorcraft operating with lift-offset rotors.

5. For the asymmetric compound operating at high-advance ratios it was observed that a low rotor RPM and a high flapping stiffness was preferred over a high RPM rotor with low flapping stiffness. The weight penalty from the higher flap frequency was found to be lower than that incurred from the heavier powerplant and transmission required to overcome the compressibility drag.

This study highlights the need to use a high-fidelity performance model as part of the sizing process for the accurate determination of vehicle. Inclusion of flap dynamics for performance calculations is necessary to accurately estimate the rotor flap frequency (a key design parameter) and the resulting fuel and power requirements of the design.

ACKNOWLEDGMENTS

The authors would like to thank Dr. Rajneesh Singh and Mr. Mike Avera of the U.S. Army Research Laboratory at Aberdeen, Maryland, for their insightful comments and suggestions.

REFERENCES

[1]Johnson, W., "A History of Rotorcraft Comprehensive Analyses," Technical report, Ames Research Center, NASA-TP-2012-216012, Moffett Field, CA, April 2012.

[2]Yeo, H., and Johnson, W., "Aeromechanics Analysis of a Heavy Lift Slowed-Rotor Compound Helicopter," *Journal of Aircraft*, Vol. 44, (2), 2007, pp. 501–508.

[3]Yeo, H., Sinsay, J.D., and Acree, C.W., Jr., "Blade Loading Criteria for Heavy Lift Tiltrotor Design," American Helicopter Society Southwest Region Technical Specialists' Meeting on Next Generation Vertical Lift Technologies, Dallas, TX, October, 2008.

[4]Anh Vu, N., Lee, Y. J., Lee, J. W., Kim, S., and Jae Chung, I., "Configuration Design and Optimisation Study of a Compound Gyroplane," *Aircraft Engineering and Aerospace Technology*, Vol. 83, (6), 2011, pp. 420–428.

[5]Avera, M., Kang, H., and Singh, R., "Comprehensive Rotorcraft Analysis for Preliminary Design and Optimization," Proceedings of the 71st Annual Forum of the American Helicopter Society, Virginia Beach, VA, May 5–7, 2015.

[6]Moodie, A. M., and Keen, E. B., and Gallaher, A. T., "Design and Assessment of a Size Constrained Advanced Tilt Rotor, Lift Offset Coaxial Compound and Winged Compound," , January 2016.

[7]David, C. V., "Heliplane," Technical Report 4,730,795, U.S. Patent, March 15, 1988.

[8]Cai, G., Dias, J., and Seneviratne, L., "A Survey of Small-Scale Unmanned Aerial Vehicles: Recent Advances and Future Development Trends," *Unmanned Systems*, Vol. 2, (2), 2004, pp. 1–25.

[9]Sartorius, S., "A Tool for Rotorcraft Pre-Design Sizing," Proceedings of the 67th Annual Forum of the American Helicopter Society, Virginia Beach, VA, May 3–5, 2011.

[10]Cumbreras, P. R., and Sartorius, S., "Feasibility Study of a Novel Asymmetric Rotorcraft Configuration: Single-Rotor Advancing Blade Concept," Presented at the 2013 International Powered Lift Conference, AIAA Aviation, Los Angeles, CA, August 12–14, 2013.

[11]Sridharan, A., Govindarajan, B. M., Nagaraj, V. T., and Chopra, I., "Design Considerations of a Lift-Offset Single Main Rotor Compound Helicopter," , January 2016.

[12]Tishchenko, M. N., Nagaraj, V. T., and Chopra, I., "Unmanned Transport Helicopters," *Journal of the American Helicopter Society*, Vol. 48, (2), April, 2003, pp. 71–79.

[13]Johnson, W., "NDARC - NASA Design and Analysis of Rotorcraft Validation and Demonstration," American Helicopter Society Aeromechanics Specialists Meeting, San Francisco, CA, January 20–22, 2010.

[14]Moodie, A.M. and Yeo, H., "Design of a Cruise-Efficient Compound Helicopter," *Journal of the American Helicopter Society*, Vol. 57, (3), 2012, pp. 1–11.

[15]Sridharan, A., *Simulation Modeling of Flight Dynamics, Control and Trajectory Optimization of Rotorcraft Towing Submerged Loads*, PhD Dissertation, Department of Aerospace Engineering, University of Maryland, College Park, MD, 2014.

[16]Passe, B., Sridharan, A., and Baeder, J. D., "Computational Investigation of Coaxial Rotor Interactional Aerodynamics in Steady Forward Flight," 33rd AIAA Applied Aerodynamics Conference, AIAA 2015-2883, Dallas, TX, 22–26 June, 2015.

[17]Peters, D. A., and He, C., "Comparison of Measured Induced Velocities with Results from a Closed-Form Finite State Wake Model in Forward Flight," Proceedings of the 45th Annual Forum of the American Helicopter Society, Boston, MA, May 22–24, 1989.

[18]Govindarajan, B. M., and Leishman, J. G., "Predictions of Rotor and Rotor/Airframe Configurational Effects on Brownout Dust Clouds," *Journal of Aircraft*, Vol. 53, (2), 2016, pp. 545–560.

[19]Leishman, J. G., *Principles of Helicopter Aerodynamics*, Cambridge University Press, New York, NY, 2006.

[20]Miklosovic, D. S., and Murraay, M. M., and Laurens, E. H., "Experimental Evaluation of Sinusoidal Leading Edges," *Journal of Aircraft*, Vol. 44, (4), 2007, pp. 1,404–1,407.

[21]Glauert, H.., "On the Horizontal Flight of a Helicopter," Technical report, ARC R&M 1157, March 1928.

[22]Glauert, H., "Airplane Propellers," *Aerodynamic Theory*, Springer, 1935, pp. 169–360.

APPENDIX

Power Calculations: Simplified Model

During design iterations, two models of different fidelity levels are available for the estimation of rotor shaft torque and engine power. The reduced-order model, implemented using momentum theory and an energy approach, does not explicitly model local effects such as varying blade geometry, tip compressibility or stall. Instead, these losses are folded into power factors that multiply the induced and profile power coefficients; see Ref. 11.

Hover: The breakdown of hover power is given by

$$\begin{aligned} P_{i_{\mathrm{H}}} &= N_{\mathrm{R}}\,\kappa_{\mathrm{H}}\frac{T^{3/2}}{\sqrt{2\rho A}} \\ P_{o_{\mathrm{H}}} &= N_{\mathrm{R}}\frac{\sigma C_{d_0}}{8}\rho A(\Omega R)^3 \\ P_{\mathrm{H}} &= \kappa_{\mathrm{int}}P_{i_{\mathrm{H}}} + P_{o_{\mathrm{H}}} \end{aligned} \tag{2}$$

where N_R is the number of rotors, ρ is the local atmospheric density, A is the rotor disk area, C_{d_0} is mean profile drag coefficient and ΩR is the hover tip speed. $P_{i,H}$, $P_{o,H}$ and P_H are the induced, profile and total power in hover, respectively. The inter-rotor interference factor κ_{int} is set to 1.0 for single rotor designs, and 1.15 for coaxial rotors.

Cruise: In forward flight (i.e., cruise), the power required is computed from the vehicle drag, which is a combination of the fuselage drag, blade drag and wing drag (if a fixed wing present). The fuselage equivalent flat-plate area (in sq.ft) is obtained from gross take-off weight and is given by

$$f = K_f \sqrt{\left(\frac{W}{1000}\right)} \tag{3}$$

where W is the take-off weight expressed in pounds, and K_f is the empirical constant set to 7.0 for utility helicopters, and between 4.0–5.0 for more streamlined designs (curve fit from Fig. 6.25 (Ref. 19)). Blade drag at the hub is estimated using a corrected disk-averaged force, $F_{x,H}$, as

$$F_{x,H} = N_R \frac{\sigma C_{d_0}}{8}(3.1\mu)\ \rho A(\Omega R)^2 \tag{4}$$

Mast Drag for Coaxials: For coaxial rotors, the mast drag is folded into the flat-plate area calculations. The mast is assumed to be a cylinder of diameter 7.5% R and a height of 20% R. A fairing with a NACA0020 is assumed. Using a fairing drag coefficient of 0.2 (Ref. 20) yields the mast flat-plate area as

$$f_{mast} = 0.003R^2 \tag{5}$$

Wing Loads: When an asymmetric fixed wing is present, the wing lift fraction is used to compute the contribution of the wing to vertical thrust. The wing lift fraction f_W is a non-dimensional metric between 0 and 1 that represents the fraction of vehicle weight carried by the fixed wing during cruise. The lower limit 0 implies all the vertical thrust is provided by the rotor, and 1 implies that the wing carries the entire vehicle weight. Using the vehicle weight generated during each fixed-point iteration, the total wing lift can be computed using the lift fraction. The wing is assumed to operate at its optimum angle of attack for minimum drag, i.e.

$$C_{L_w} = C_{L_{opt}} = \sqrt{\frac{C_{D_0}}{K}} \tag{6}$$

where $K = 1/(\pi\ \mathrm{AR}_{wing}\ \mathrm{e})$. Therefore, the optimum wing area S_{wing} is given by

$$S_{wing} = \frac{f_W W_{cr}}{0.5\rho V_\infty^2 C_{L_{opt}}} \tag{7}$$

The wing drag D_{wing} is

$$\begin{aligned} D_{wing} &= 0.5\rho V_\infty^2 S_{wing}(KC_{L_{opt}}^2 + C_{D_{0w}}) \\ &= 0.5\rho V_\infty^2 S_{wing}(2C_{D_{0w}}) \end{aligned} \tag{8}$$

V_∞ is the forward flight speed, $C_{d_{0W}}$ is the mean drag profile coefficient of the wing and e is the Oswald's efficiency factor. Using the aspect ratio of the wing, AR_{wing}, the wing span, b_{wing}, and mean wing chord, c_{wing} are computed as

$$b_{wing} = \sqrt{\mathrm{AR}_{wing}\ \mathrm{S}_{wing}} \tag{9}$$

$$c_{wing} = S_{wing}/b_{wing} \tag{10}$$

Therefore, from Eqs. 3, 4, 5 and 8, the total drag is given by

$$D = \frac{1}{2}\rho V_\infty^2(f + f_{mast}) + F_{x,H} + D_{wing} \tag{11}$$

Rotor Shaft Tilt in Cruise: To compute rotor induced power, an estimate of the shaft tilt is necessary for use in the uniform inflow iteration expression. The rotor tip-path-plane is assumed to be tilted back by 0.5°, so that the thrust vector is dominantly used to counteract gravity. Since a small component of the thrust may produce additional hub drag, Eq. 11 is modified to include the component of rotor shaft thrust along the free-stream velocity direction. The total propeller thrust is then given by

$$T_{prop} = \frac{1}{2}\rho V_\infty^2 f + F_{x,H} + D_{wing} - N_R T \sin\alpha_{TPP} \tag{12}$$

The propeller power is estimated from the required thrust, cruise speed and propulsive efficiency as

$$P_{prop} = \frac{T_{prop} V_\infty}{\eta_P} \tag{13}$$

Rotor Power in Cruise: In high-speed cruise, a tip Mach number limit is imposed by altering the rotor RPM so that

$$\Omega_{cr} R \leq M_{lim} a_{cr} - V_\infty \tag{14}$$

where a_{cr} is the speed of sound at cruise altitude. The total inflow for all rotors operating in edgewise flight is obtained through fixed-point iterations for the inflow equation as derived by Glauert (Refs. 21, 22)

$$\lambda = \mu \tan\alpha_{TPP} + \frac{C_T}{2\sqrt{\mu^2 + \lambda^2}} \tag{15}$$

The total inflow ratio, obtained at the end of convergence, is used to calculate the total induced power of all rotors, $P_{i,cr}$ as

$$P_{i,cr} = N_R\ \kappa_C\ C_T \lambda\ \rho A(\Omega_{cr} R)^3 \tag{16}$$

The profile power, $P_{o,cr}$, needed to rotate the blades and overcome torque due to airfoil section drag in edgewise flight is given by

$$P_{o,cr} = N_R \frac{\sigma C_{d_0}}{8}(1 + 1.55\mu^2)\rho A(\Omega_{cr} R)^3 \tag{17}$$

The total mechanical power, P_{total}, needed to turn the rotor(s) and propeller is then given by

$$P_{total} = P_{i,cr} + P_{o,cr} + P_{prop} \tag{18}$$